

# A Nonlinear Observer for Air-Velocity and Attitude Estimation Using Pitot and Barometric Measurements\*

Nyoba Tchonkeu, Melone \* Berkane, Soulaimane \*\*  
Hamel, Tarek \*\*\*

\* University of Quebec in Outaouais, Gatineau, QC J8X3X7, Canada,  
(e-mail: nyom01@uqo.ca).

\*\* University of Quebec in Outaouais, Gatineau, QC J8X3X7 and  
Lakehead University, Thunder Bay, ON P7B 5E1, Canada, (e-mail:  
soulaimane.berkane@uqo.ca).

\*\*\* I3S-UniCA-CNRS, University Côte d'Azur and the Institut  
Universitaire de France, 06903 Sophia Antipolis, France, (e-mail:  
thamel@i3s.unice.fr).

**Abstract:** This paper addresses the problem of estimating air velocity and full attitude for unmanned aerial vehicles (UAVs) in GNSS-denied environments using minimal onboard sensing—an interesting and practically relevant challenge for UAV navigation. The contribution of the paper is twofold: (i) an observability analysis establishing the conditions for uniform observability (UO), which are useful for trajectory planning and motion control of the UAV; and (ii) the design of a nonlinear observer on  $\text{SO}(3) \times \mathbb{R}^3 \times \mathbb{R}$  that incorporates pitot-tube, barometric altitude, and magnetometer measurements as outputs, with IMU data used as inputs, within a unified framework. Simulation results are presented to confirm the convergence and robustness of the proposed design, including under minimally excited trajectories.

**Keywords:** UAVs; Autonomous Navigation; Nonlinear observers and filter design; GNSS-denied; Air velocity; Barometer; Magnetometer; IMU.

## 1. INTRODUCTION

Robust estimation of air velocity and attitude is fundamental for the safe and autonomous operation of UAVs. The challenge is particularly acute in GNSS-denied environments such as urban canyons or contested airspaces, where satellite-based signals are unavailable or unreliable. Under such constraints, UAVs must rely on onboard (typically lightweight) sensors, and the design of observers capable of delivering accurate estimates with minimal instrumentation remains a central research problem.

Several authors have addressed the attitude estimation problem from inertial measurement units (IMUs). Nonlinear complementary filter on  $\text{SO}(3)$  (Mahony et al., 2008), geometric observers formulations (Lageman et al., 2008; Barczyk and Lynch, 2012), and symmetry-preserving observers approaches (Bonnabel et al., 2008) have demonstrated robust performance when aided by magnetometer or GNSS measurements. However, for fixed-wing UAVs, the accelerometer measures both gravity and aerodynamic forces, invalidating the gravity-only assumption and causing attitude observers to misinterpret dynamic loads as reference vectors (Mahony et al., 2008), thereby reducing robustness during maneuvering flight. This limita-

tion has motivated the development of velocity-aided attitude (VAA) observers, which uses velocity information to enhance observability. Examples include observers using GNSS-derived inertial velocity (Hua et al., 2016; Hansen et al., 2017; Hua et al., 2017; Grip et al., 2013; Benallegue et al., 2023; Berkane and Tayebi, 2017) or Doppler radar (Troni and Whitcomb, 2013). While effective, such methods are constrained by cost, hardware demands, and GNSS vulnerabilities, limiting their use on lightweight aerial platforms.

These constraints have increased the use of Pitot-based sensing in small UAVs. Pitot systems provide lightweight and direct measurements of specific components of the body-frame air velocity and are therefore standard equipment on fixed-wing platforms. Early approaches fused Pitot, IMU, and aerodynamic models (Lie, 2014; Borup et al., 2016), but accuracy depended strongly on aerodynamic parameters that are difficult to calibrate for small airframes. To mitigate this sensitivity, recent works have incorporated Pitot measurements directly into observer design (Sun et al., 2019; Johansen et al., 2015), thereby reducing reliance on uncertain aerodynamic models. Oliveira et al. (de Oliveira et al., 2024) further advanced this direction by proposing a Riccati–nonlinear observer on  $\text{SO}(3) \times \mathbb{R}^3$  for joint air-velocity and the gravitational direction estimation in GNSS-denied flight, and establishing the first rigorous local stability guarantees for such architectures. Owing to the sensing configuration, the system retains a

\* This work was supported by the "Grands Fonds Marins" Project Deep-C, and the ASTRID ANR project ASCAR. This research work is also supported in part by NSERC-DG RGPIN-2020-04759 and Fonds de recherche du Québec (FRQ).

structural yaw ambiguity and satisfies uniform observability only under sufficiently rich persistent excitation.

On the other hand, barometer measurements are widely available on most UAV platforms and, when properly incorporated, can relax the observability requirements of Pitot–IMU–based architectures. To this end, we extend the nonlinear observer framework of de Oliveira et al. (2024) by incorporating barometric altitude and magnetometer measurements. The barometer, routinely embedded in autopilot systems, provides continuous pressure-based altitude measurements and has long been used for vertical state estimation in fixed-wing UAVs (Mahony et al., 2011). It is commonly fused with GNSS/INS for height stabilization (Borup et al., 2016), and recent studies have indicated its potential to enhance attitude estimation in GNSS-denied conditions (Tchonkeu et al., 2025). The magnetometer supplies a global directional reference, enabling full attitude estimation (Bryne et al., 2017; Tchonkeu et al., 2025). In particular, we extend the system with a scalar altitude state that couples the original dynamics (attitude and air velocity) with the barometric measurement. We assume that the vertical wind velocity is negligible, which is standard in the absence of dedicated wind-sensing instrumentation and allows the barometric measurement to be consistently incorporated into the model. We then propose a nonlinear observer, based on the Riccati–observer framework of Hamel and Samson (2017), whose linearized error dynamics admit a bounded state matrix. Under suitable observability conditions, this property enables establishing local exponential stability of the estimation errors.

The remainder of the paper is organized as follows. Section 2 introduces notation and mathematical preliminaries. Section 3 formulates the estimation problem. Section 4 presents the proposed observer, while Section 5 provides the associated observability and stability analysis. Implementation aspects are discussed in Section 6, followed by simulation results in Section 7 and concluding remarks in Section 8.

## 2. PRELIMINARY MATERIAL

We denote by  $\mathbb{R}$  and  $\mathbb{R}_+$  the sets of real and nonnegative real numbers, respectively. The  $n$ -dimensional Euclidean space is denoted by  $\mathbb{R}^n$ . The Euclidean inner product of two vectors  $x, y \in \mathbb{R}^n$  is defined as  $\langle x, y \rangle = x^\top y$ . The associated Euclidean norm of a vector  $x \in \mathbb{R}^n$  is  $|x| = \sqrt{x^\top x}$ . Furthermore, we denote by  $\mathbb{R}^{m \times n}$  the set of real  $m \times n$  matrices. The set of  $n \times n$  positive definite matrices is denoted by  $\mathcal{S}^+(n)$ , and the identity matrix is denoted by  $I_n \in \mathbb{R}^{n \times n}$ . Given two matrices  $A, B \in \mathbb{R}^{m \times n}$ , the Euclidean matrix inner product is defined as  $\langle A, B \rangle = \text{tr}(A^\top B)$ , and the Frobenius norm of  $A \in \mathbb{R}^{n \times n}$  is given by  $\|A\| = \sqrt{\langle A, A \rangle}$ . The unit sphere  $\mathbb{S}^2 := \{\eta \in \mathbb{R}^3 \mid |\eta| = 1\} \subset \mathbb{R}^3$  denotes the set of unit 3D vectors and forms a smooth submanifold of  $\mathbb{R}^3$ . The special orthogonal group of 3D rotations is denoted by  $\text{SO}(3) := \{R \in \mathbb{R}^{3 \times 3} \mid RR^\top = R^\top R = I_3, \det(R) = 1\}$ . The Lie algebra of  $\text{SO}(3)$  is  $\mathfrak{so}(3) := \{\Omega \in \mathbb{R}^{3 \times 3} \mid \Omega^\top = -\Omega\}$ , isomorphic to  $\mathbb{R}^3$  via the skew-symmetric operator  $(\cdot)^\times : \mathbb{R}^3 \rightarrow \mathfrak{so}(3)$ , defined such that  $u \times v = u^\times v$  for all  $u, v \in \mathbb{R}^3$ . The exponential map  $\exp : \mathfrak{so}(3) \rightarrow \text{SO}(3)$

defines a local diffeomorphism from a neighborhood of  $0 \in \mathfrak{so}(3)$  to a neighborhood of  $I_3 \in \text{SO}(3)$ . This enables the composition map  $\exp \circ (\cdot)^\times : \mathbb{R}^3 \rightarrow \text{SO}(3)$ , which is given by the following Rodrigues' formula (Ma et al., 2004):

$$\exp([\theta]^\times) = I_3 - \frac{\sin(\|\theta\|)}{\|\theta\|} [\theta]^\times + \frac{1 - \cos(\|\theta\|)}{\|\theta\|^2} ([\theta]^\times)^2. \quad (1)$$

## 3. PROBLEM DESCRIPTION

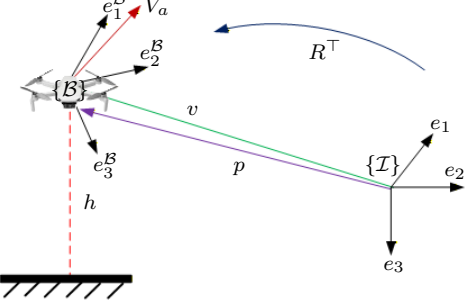


Fig. 1. We assume a vehicle equipped with an IMU, a set of  $m$  Pitot tubes measuring components of the air velocity  $V_a$ , and a barometer measuring the height  $h$ .

Consider a fixed-wing aerial vehicle equipped with an IMU (gyroscopes and accelerometers), a set of  $m$  Pitot probes, and a barometric pressure sensor (see fig. 1).

Let  $R \in \text{SO}(3)$  denote the rotation matrix from the vehicle body-fixed frame  $\mathcal{B}$  to the inertial frame  $\mathcal{I}$ , and let  $\omega \in \mathbb{R}^3$  and  $\mathbf{a} \in \mathbb{R}^3$  be the body angular velocity and the linear specific acceleration measured by IMU, respectively. The position and linear velocity of the rigid body, expressed in the inertial frame  $\mathcal{I}$ , are denoted by  $p \in \mathbb{R}^3$  and  $v \in \mathbb{R}^3$ , respectively. The gravitational acceleration is expressed in the inertial frame by  $\mathbf{g} = g\mathbf{e}_3 \in \mathbb{R}^3$ , where  $\mathbf{e}_3 = [0 \ 0 \ 1]^\top \in \mathbb{S}^2$  denotes the standard gravity direction, and  $g \approx 9.81 \text{ m/s}^2$  is the gravity constant. The vehicle's translational and rotational kinematics are given by

$$\dot{v} = R\mathbf{a} + g\mathbf{e}_3,$$

$$\dot{R} = R\omega^\times.$$

Let  $v_w \in \mathbb{R}^3$  be the inertial wind velocity. The vehicle air-velocity in inertial and body frames are  $v_a = v - v_w$  and  $V_a = R^\top v_a$ , respectively. Assuming a constant bounded wind velocity throughout the flight ( $\dot{v}_w \approx 0$ ), one obtains  $\dot{v}_a = \dot{v}$ . Hence, the air-velocity and attitude dynamics become :

$$\dot{v}_a = R\mathbf{a} + g\mathbf{e}_3, \quad (2)$$

$$\dot{R} = R\omega^\times. \quad (3)$$

The vehicle is equipped with  $m$  calibrated Pitot probes. Each probe measures the scalar projection of the air-velocity  $V_a$  along a known body-fixed direction  $b_i \in \mathbb{S}^2$ :

$$y_{p,i} = b_i^\top V_a + n_{p,i} = b_i^\top R^\top v_a + n_{p,i}, \quad (4)$$

where  $n_{p,i} \sim \mathcal{N}(0, \sigma_{p,i}^2) \in \mathbb{R}$  is zero-mean noise. Collectively, multi-probe Pitot system vector is modeled as

$$y_p = B^\top V_a + n_p, \quad B = [b_1 \cdots b_m] \in \mathbb{R}^{3 \times m}, \quad (5)$$

where  $n_p = [n_{p,1} \cdots n_{p,m}]^\top \in \mathbb{R}^m$ . To enhance the observability of the vehicle's motion, a scalar altitude

variable is introduced as  $h := \mathbf{e}_3^\top p \in \mathbb{R}$ , which is measured by the barometric sensor modeled:

$$y_b = h + n_b, \quad (6)$$

where  $n_b \sim \mathcal{N}(0, \sigma_b^2) \in \mathbb{R}$  is zero-mean noise.

We also assume that the vertical wind velocity,  $\mathbf{e}_3^\top v_w$ , is negligible, as it is typically much smaller than horizontal winds in low-altitude UAV operations. Furthermore, we assume that the IMU includes a magnetometer. The measured Earth's magnetic field in the body-frame  $\mathbf{m}_B \in \mathbb{S}^2$  is then modeled as

$$\mathbf{m}_B = R^\top m_I + n_m, \quad (7)$$

where  $m_I \in \mathbb{S}^2$  is the known magnetic field vector expressed in the inertial frame and  $n_m \sim \mathcal{N}(0, \sigma_m^2) \in \mathbb{R}^3$  is zero-mean noise. The objective is to estimate the full air-velocity and attitude states from these measurements, exploiting the altitude and heading information to enhance the overall system observability and estimation performance of the coupled air-velocity–attitude dynamics described by (2) and (3).

#### 4. PROPOSED OBSERVER DESIGN

This section presents the design of a barometric-augmented observer that extends the local framework of de Oliveira et al. (2024) to include barometric and magnetic measurements. The proposed architecture comprises a local Riccati equation (19) that processes the linearized attitude–air-velocity–altitude error dynamics to generate innovation terms (20), which are then injected into a nonlinear observer (10) on  $\text{SO}(3) \times \mathbb{R}^3 \times \mathbb{R}$  to estimate the full orientation, air-velocity, and altitude. The overall architecture is illustrated in fig. 2.

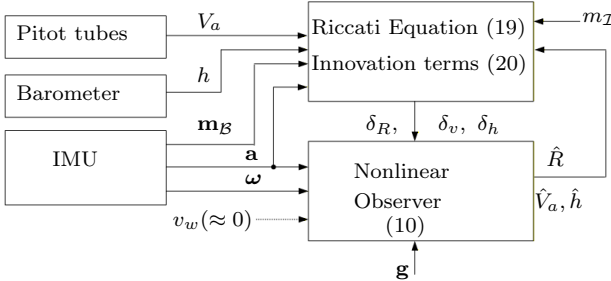


Fig. 2. Overall structure of the proposed nonlinear observer.

From (2) and (3), the body-frame air-velocity dynamics follow directly from de Oliveira et al. (2024) and are given by:

$$\dot{V}_a = -\boldsymbol{\omega}^\times V_a + gR^\top \mathbf{e}_3 + \mathbf{a}. \quad (8)$$

The inertial altitude is defined as  $h := \mathbf{e}_3^\top p$ . Since  $\dot{p} = v \approx v_a$ , it follows that

$$\dot{h} = \mathbf{e}_3^\top v_a = \mathbf{e}_3^\top RV_a. \quad (9)$$

Combining (3) and (8)–(9), we propose the following nonlinear observer on  $\text{SO}(3) \times \mathbb{R}^3 \times \mathbb{R}$ , whose structure consists of a copy of the system dynamics augmented with suitable innovation terms:

$$\begin{cases} \dot{\hat{R}} = \hat{R}\boldsymbol{\omega}^\times - \delta_R^\times \hat{R}, & \hat{R}(0) \in \text{SO}(3), \\ \dot{\hat{V}}_a = -\boldsymbol{\omega}^\times \hat{V}_a + g\hat{R}^\top \mathbf{e}_3 + \mathbf{a} - \hat{R}^\top \delta_v + \hat{R}^\top \delta_R^\times \hat{R}\hat{V}_a, \\ \dot{\hat{h}} = \mathbf{e}_3^\top \hat{R}\hat{V}_a - \delta_h, \end{cases} \quad (10)$$

where  $\hat{R} \in \text{SO}(3)$  denotes the estimate of  $R$ ,  $\hat{V}_a \in \mathbb{R}^3$  the estimate of  $V_a$ , and  $\hat{h} \in \mathbb{R}$  the estimate of  $h$ .  $\delta_R \in \mathbb{R}^3$ ,  $\delta_v \in \mathbb{R}^3$ ,  $\delta_h \in \mathbb{R}$  are the correction terms, which will be determined from the linearization process below.

Let  $\tilde{R} := RR^\top$ ,  $\tilde{v}_a := RV_a - \hat{R}\hat{V}_a$ , and  $\tilde{h} := h - \hat{h}$  denote, respectively, the attitude, inertial air-velocity, and barometric errors. From (3) and (8)–(10), one obtains the following nonlinear error dynamics:

$$\dot{\tilde{R}} = \tilde{R}\delta_R^\times, \quad (11a)$$

$$\dot{\tilde{v}}_a = (\tilde{R} - I_3)\hat{R}\mathbf{a} + \delta_v, \quad (11b)$$

$$\dot{\tilde{h}} = \mathbf{e}_3^\top \tilde{v}_a + \delta_h, \quad (11c)$$

To linearize (11), we express  $\tilde{R}$  in terms of its associated unit quaternion  $\tilde{\mathbf{q}} := (\tilde{q}_0, \tilde{\mathbf{q}})$ , using Rodrigues' formula (Ma et al., 2004):

$$\tilde{R} = I_3 + 2\tilde{q}^\times(\tilde{q}_0 I_3 + \tilde{q}^\times), \quad (12)$$

where for a rotation by an angle  $\theta$  about a unit axis  $\mathbf{u} \in \mathbb{S}^2$ , one has  $\tilde{q}_0 = \cos(\theta/2)$  and  $\tilde{q} = \mathbf{u}\sin(\theta/2)$ . For small attitude errors ( $\delta\theta$ ),  $\|\tilde{q}\| \ll 1$  and  $\tilde{q} = \mathbf{u}\delta\theta/2$ . Then, one obtains the second-order approximation  $\tilde{q}_0 \approx 1 + \mathcal{O}(\|\tilde{q}\|^2)$ . Substituting this into (12), yields

$$\tilde{R} = I_3 + (2\text{sign}(\tilde{q}_0)\tilde{q})^\times + \mathcal{O}(\|\tilde{q}\|^2).$$

By defining  $\tilde{\lambda} = 2\text{sign}(\tilde{q}_0)\tilde{q} \in \mathbb{R}^3$  with  $\|\tilde{\lambda}\| = \mathcal{O}(\|\tilde{q}\|)$ , the first order approximation of attitude error becomes

$$\tilde{R} = I_3 + \tilde{\lambda}^\times + \mathcal{O}(\|\tilde{\lambda}\|^2). \quad (13)$$

Exploiting the above first order approximation, one can rewrite (11), as follows:

$$\dot{\tilde{\lambda}} = \delta_R + \mathcal{O}(\|\tilde{\lambda}\|\|\delta_R\|), \quad (14a)$$

$$\dot{\tilde{v}}_a = -(\hat{R}\mathbf{a})^\times \tilde{\lambda} + \delta_v + \mathcal{O}(\|\tilde{\lambda}\|^2), \quad (14b)$$

$$\dot{\tilde{h}} = \mathbf{e}_3^\top \tilde{v}_a + \delta_h. \quad (14c)$$

For the output, we define the estimated Pitot, barometer, and magnetometer measurements, respectively, as  $\hat{y}_p := B^\top \hat{V}_a$ ,  $\hat{y}_b := \hat{h}$ , and  $\hat{y}_m := \hat{R}\mathbf{m}_B$ . In view of (5)–(7) and (13), the output errors  $\tilde{y}_p := y_p - \hat{y}_p$ ,  $\tilde{y}_b := y_b - \hat{y}_b$ , and  $\tilde{y}_m := m_I - \hat{y}_m$  satisfy

$$\tilde{y}_p = B^\top \hat{R}^\top (\hat{R}\hat{V}_a)^\times \tilde{\lambda} + B^\top \hat{R}^\top \tilde{v}_a + \mathcal{O}(\|\tilde{\lambda}\|\|\tilde{v}_a\| + \|\tilde{\lambda}\|^2),$$

$$\tilde{y}_m = -(m_I)^\times \tilde{\lambda} + \mathcal{O}(\|\tilde{\lambda}\|^2),$$

$$\tilde{y}_b = \tilde{h}.$$

Let  $x := [\tilde{\lambda}^\top \tilde{v}_a^\top \tilde{h}]^\top \in \mathbb{R}^7$ ,  $u(t) := [\delta_R^\top \delta_v^\top \delta_h]^\top$ , and  $y := [\tilde{y}_p^\top \tilde{y}_m^\top \tilde{y}_b]^\top \in \mathbb{R}^{m+4}$ . The local error dynamics admit the linear time-varying (LTV) representation

$$\dot{x} = A(t)x + u(t) + \mathcal{O}(\|x_1\|\|u\| + \|x_1\|^2), \quad (15a)$$

$$y = C(t)x + \mathcal{O}(\|x_1\|\|x_2\| + \|x_1\|^2). \quad (15b)$$

The matrices  $A(t)$  and  $C(t)$  in (15) are given explicitly by

$$A(\hat{R}(t)) = \begin{bmatrix} \mathbf{0}_{3 \times 3} & \mathbf{0}_{3 \times 3} & \mathbf{0}_{3 \times 1} \\ -(\hat{R}\mathbf{a})^\times & \mathbf{0}_{3 \times 3} & \mathbf{0}_{3 \times 1} \\ \mathbf{0}_{1 \times 3} & \mathbf{e}_3^\top & 0 \end{bmatrix}, \quad (16)$$

$$C(\hat{R}(t), \hat{V}_a(t)) = \begin{bmatrix} B^\top \hat{R}^\top (\hat{R} \hat{V}_a)^\times & B^\top \hat{R}^\top & \mathbf{0}_{m \times 1} \\ -(m_I)^\times & \mathbf{0}_{3 \times 3} & \mathbf{0}_{3 \times 1} \\ \mathbf{0}_{1 \times 3} & \mathbf{0}_{1 \times 3} & 1 \end{bmatrix}. \quad (17)$$

To determine the innovation terms  $\delta_R$ ,  $\delta_v$ , and  $\delta_h$ , we design a local Kalman–Bucy-type gain  $K(t)$  for (15). Using the innovation input  $u(t) = -K(t)y(t)$ , the closed-loop error dynamics become

$$\dot{x} = (A - K(t)C(t))x + \mathcal{O}(\|x_1\| \|Ky\| + \|x_1\|^2) - K(t) \mathcal{O}(\|x_1\| \|x_2\| + \|x_1\|^2), \quad (18)$$

where  $K(t) = P(t)C^\top(t)Q \in \mathbb{R}^{7 \times (m+4)}$  and  $P(t)$  solves the continuous-time Riccati equation (CRE)

$$\dot{P} = A(t)P + PA^\top(t) - PC^\top(t)Q C(t)P + S, \quad (19)$$

with  $P(0) > 0$ . The matrices  $Q > 0$  and  $S > 0$  are symmetric positive definite, where  $Q$  encodes the sensor precisions ( $Q_p$  for the Pitot,  $Q_m$  for the magnetometer, and  $Q_b$  for the barometer), while  $S$  plays the role of the process noise covariance. We decompose

$$K(t) = [K_{\delta_R}(t)^\top \ K_{\delta_v}(t)^\top \ K_{\delta_h}(t)^\top]^\top,$$

with  $K_{\delta_R} \in \mathbb{R}^{3 \times (m+4)}$ ,  $K_{\delta_v} \in \mathbb{R}^{3 \times (m+4)}$ , and  $K_{\delta_h} \in \mathbb{R}^{1 \times (m+4)}$ . Then, using the definition of  $u(t)$ , the Riccati solution yields the innovation terms

$$\delta_R(t) = -K_{\delta_R}(t) y(t), \quad (20a)$$

$$\delta_v(t) = -K_{\delta_v}(t) y(t), \quad (20b)$$

$$\delta_h(t) = -K_{\delta_h}(t) y(t). \quad (20c)$$

The stability and convergence properties of (20) are fundamentally linked to the well-posedness of the CRE, which requires the UO of the associated LTV model. Let us define the matrices  $A^*(t) = A(R(t))$  and  $C^*(t) = C(R(t), V_a(t))$  associated with the true trajectory. The UO of the linearized error system in (15) inherits from the UO of  $(A^*(t), C^*(t))$ . According to Theorem 3.1 of Hamel and Samson (2017), if the pair  $(A^*(t), C^*(t))$  is uniformly observable, the CRE in (19) admits a unique, bounded, and positive-definite solution  $P(t)$  for all  $t \geq 0$ . As a consequence, the local error  $x$  of (15) decays exponentially to the origin, with the rate of convergence tuned by  $Q$  larger than some positive matrix and  $S > 0$ , ensuring stability and convergence of the nonlinear observer in (10).

## 5. OBSERVABILITY AND STABILITY ANALYSIS

Consider the LTV system in (15). By definition from Besançon (2007), the system (15) or pair  $(A(t), C(t))$  is *uniformly observable* if there exist constants  $\delta, \mu > 0$  such that, for all  $t \geq 0$ ,

$$W(t, t+\delta) := \frac{1}{\delta} \int_t^{t+\delta} \Phi^\top(s, t) C^\top(s) C(s) \Phi(s, t) ds \geq \mu I_n, \quad (21)$$

where  $\Phi(s, t)$  is the state transition matrix such that

$$\frac{d}{dt} \Phi(s, t) = A(t) \Phi(s, t), \quad \Phi(t, t) = I_n, \quad \forall s \geq t. \quad (22)$$

$W(t, t + \delta)$  is called the *observability Gramian* of the system.

The purpose of the following lemma is to establish trajectory-dependent sufficient conditions for the uniform observability of the pair  $(A^*, C^*)$  associated with the true

system. Hence, for a given trajectory, these conditions can be verified without explicitly computing the corresponding observability Gramian.

**Lemma 1.** Assume that the body-frame linear acceleration  $\mathbf{a}(t)$ , the angular velocity  $\boldsymbol{\omega}(t)$ , and the air-velocity  $V_a(t)$  are continuous and uniformly bounded. Moreover, assume that vectors  $m_I$  and  $\mathbf{e}_3$  are non-collinear. Let  $J = [\mathbf{e}_1 \ \mathbf{e}_2] \in \mathbb{R}^{3 \times 2}$ , where  $\mathbf{e}_1$  and  $\mathbf{e}_2$  denote the first two canonical basis vectors of  $\mathbb{R}^3$ . Define  $\Pi(t) = B^\top R(t)J$  and  $a_\pi(t) = \mathbf{e}_3^\top (R(t)\mathbf{a}(t))^\times J$ . Assume there exist  $\bar{\delta} > 0$  and  $\bar{\mu}_1, \bar{\mu}_2 > 0$  such that, for all  $t \geq 0$ ,

$$\frac{1}{\bar{\delta}} \int_t^{t+\bar{\delta}} \Pi(s)^\top \Pi(s) ds \geq \bar{\mu}_1 I_2, \quad (23)$$

and

$$\frac{1}{\bar{\delta}} \int_t^{t+\bar{\delta}} a_\pi(s)^\top a_\pi(s) ds \geq \bar{\mu}_2 I_2. \quad (24)$$

Then the time-varying pair  $(A^*(t), C^*(t))$  is uniformly observable.

**Proof.** See Appendix A.

The excitation requirements of Lemma 1 differ fundamentally from the Pitot-only setting of de Oliveira et al. (2024). With a single Pitot probe, de Oliveira et al. (2024) requires both yaw and pitch excitation to ensure observability, since the PE condition is imposed on the full matrix  $B^\top R^\top$  and no absolute heading is available. In contrast, the present formulation—with magnetometer and barometer—separates the excitation across sensing channels. The Pitot contribution enters only through the horizontal projection  $B^\top R(t)J$ , so with  $b_1 = \mathbf{e}_1$  the required motion reduces to *yaw excitation only*. Moreover, when two probes are available with linearly independent horizontal projections,  $B^\top R(t)J$  already has full rank in the horizontal plane, and the Pitot-induced PE condition can be satisfied *without any motion*, whereas the Pitot-only case of de Oliveira et al. (2024) requires three probes for the same effect. Finally, the baro-induced term  $a_\pi(t)$  contributes vertical excitation whenever the inertial acceleration possesses a horizontal component—purely vertical acceleration does not help. Altogether, the PE conditions (23)–(24) reorganize the needed excitation across horizontal Pitot geometry, horizontal components of the inertial specific force, and absolute yaw from the magnetometer. The following theorem follows directly from this uniform observability property.

**Theorem 2.** Consider the system (2)–(7) along with the closed loop error (18) and the nonlinear observer (10), with the innovation inputs (20), and  $P(t)$  the symmetric positive definite matrix solution to the CRE (19). Assume the pair  $(A^*(t), C^*(t))$  is uniformly observable, then the origin of the closed error dynamic (18) is locally exponentially stable.

**Proof.** Consider the Lyapunov function  $L := x^\top P^{-1} x$ . Using the CRE in (19) and the innovation terms in (20), one obtains (see Sastry (1999))

$$\dot{L} = -\frac{1}{2} x^\top (C^\top(t) Q C(t) + P^{-1}(t) S P^{-1}(t)) x + \mathcal{O}(\|x\|^3, \|P\|^{-2}). \quad (25)$$

The quadratic term in (25) is strictly dissipative provided  $P(t)$  and  $P^{-1}(t)$  are uniformly bounded and positive def-

inite. By Lemma 1, the pair  $(A(t), C(t))$  in (15) is uniformly observable. Hence, along the equilibrium trajectory (i.e., when  $\Pi(t) = B^\top R(t)J$  and  $a_\pi(t) = \mathbf{e}_3^\top (R(t)\mathbf{a}(t))^\times J$ ), the associated Riccati solution is bounded and well-conditioned (see Prop. 17 of de Oliveira et al. (2024)). Furthermore, by Theorem 3.1 of Hamel and Samson, 2017 or Prop. 25 of Barrau and Bonnabel (2019), it follows that for  $Q > 0$  and  $S > 0$ , the solution  $P(t)$  of the CRE in (19) exists along bounded trajectories and remains uniformly bounded and positive definite. As a result, both  $P(t)$  and  $P^{-1}(t)$  are uniformly bounded, so the remainder term  $\mathcal{O}(\|x\|^3, \|P\|^{-2})$  can be dominated by the strictly negative quadratic term in a sufficiently small neighborhood of the origin. Consequently, there exists  $\gamma > 0$  such that  $\dot{L} \leq -\gamma L$ , which implies  $\|x(t)\| \leq ce^{-\gamma(t-t_0)}\|x(t_0)\|$ ,  $\forall t \geq t_0$ , for some  $c > 0$ . Hence, the origin is a locally exponentially stable equilibrium for the closed-loop error dynamics in (18).

Theorem 2 ensures local exponential convergence whenever the excitation conditions of Lemma 1 are satisfied. When  $m \geq 3$ , the probe geometry provides sufficient horizontal excitation through  $B^\top R(t)J$  without requiring specific vehicle motion (see de Oliveira et al. (2024)). For  $m = 2$ , convergence can also occur without motion when the two probes have linearly independent horizontal projections, since the vertical direction is recovered through the baro-acceleration coupling. When only a single probe is available, horizontal excitation must arise from the vehicle motion, and in this case, yaw excitation is sufficient thanks to the magnetometer and barometric measurements. Thus, exponential convergence may be achieved either through probe geometry or through horizontal excitation induced by the vehicle dynamics.

## 6. DISCRETE TIME IMPLEMENTATION

The proposed observer is implemented at the IMU sampling period  $T$ . Over each interval  $[t_k, t_{k+1}]$ , we assume the measured acceleration  $\mathbf{a}_k$ , the angular velocity  $\boldsymbol{\omega}_k$ , and the body-frame air-velocity  $V_{a,k}$  are constant (see Bryne et al. (2017)). Moreover, we assume the discrete process noise  $S_{d,k} \approx S_k T$ , the estimated air-velocity  $\hat{V}_a(t) \approx \hat{V}_{a,k}$ , and the estimated attitude  $\hat{R}(t) \approx \hat{R}_k$  for  $t \in [t_k, t_{k+1}]$ . Using these assumptions, a first-order discretization of the continuous-time state matrix  $A(t)$  yields

$$A_{d,k} \approx \begin{bmatrix} I_3 & \mathbf{0}_{3 \times 3} & \mathbf{0}_{3 \times 1} \\ -T(\hat{R}_k \mathbf{a}_k)^\times & I_3 & \mathbf{0}_{3 \times 1} \\ \mathbf{0}_{1 \times 3} & T \mathbf{e}_3^\top & 1 \end{bmatrix}. \quad (26)$$

The continuous-time output matrix  $C(t)$  is sampled at the measurement timestamp as follows

$$C_k = [C_{p,k}^\top, C_{m,k}^\top, C_{b,k}^\top]^\top \quad (27)$$

where

$$C_{p,k} = [B^\top \hat{R}_k^\top (\hat{R}_k \hat{V}_{a,k})^\times B^\top \hat{R}_k^\top \mathbf{0}_{m \times 1}], \quad (28)$$

$$C_{m,k} = [-(m_I)^\times \mathbf{0}_{3 \times 3} \mathbf{0}_{3 \times 1}]. \quad (29)$$

$$C_{b,k} = [\mathbf{0}_{1 \times 3} \mathbf{0}_{1 \times 3} 1]. \quad (30)$$

The resulting discrete-time observer, summarized in Algorithm 1, follows the standard correction–prediction structure with the above state and output matrices. The nonlinear observer (10) is discretized at the IMU frequency using

---

**Algorithm 1** Discrete-Time Implementation of the proposed observer

---

**Inputs:**  $x_{0|0}, P_{0|0}, \hat{R}_0, \hat{V}_{a,0}, \hat{h}_0; g_k, \mathbf{a}_k, \boldsymbol{\omega}_k, \mathbf{m}_{\mathcal{B}_k}; y_{p,k}; y_{m,k}; y_{b,k}; T; Q_k; S_k; v_w \approx 0; B = b_1$ .  
**Outputs:**  $\hat{R}_k, \hat{V}_{a,k}, \hat{h}_k, \forall k \in \mathbb{N}$

- 1: **for** each time  $k \geq 0$  **do**
- 2:   **if** IMU data  $\mathbf{a}_k, \boldsymbol{\omega}_k$  is available **then**
- 3:      $A_{d,k} \leftarrow (26)$ ;  $S_{d,k} \leftarrow S_k T$ ;
- 4:      $P_{k+1|k} \leftarrow A_{d,k} P_{k|k} A_{d,k}^\top + S_{d,k}$ .
- 5:   **end if**
- 6:   **if**  $y_{p,k}, y_{m,k}$ , and  $y_{b,k}$  are all available **then**
- 7:      $C_{p,k} \leftarrow (28)$ ;  $C_{m,k} \leftarrow (29)$ ;  $C_{b,k} \leftarrow (30)$ ;  
 $C_k \leftarrow (27)$ ;
- 8:      $y_k \leftarrow \begin{bmatrix} y_{p,k} - B^\top \hat{V}_{a,k} \\ y_{m,k} - \hat{R}_k \mathbf{m}_{\mathcal{B}_k} \\ y_{b,k} - \hat{h}_k \end{bmatrix}$ ;
- 9:      $Q_k \leftarrow \text{blkdiag}(Q_{p,k}, Q_{m,k}, Q_{b,k})$ .
- 10:   **else if** Barometer measurement is available **then**
- 11:      $C_{b,k} \leftarrow (30)$ ;  $C_k \leftarrow C_{b,k}$ ;
- 12:      $y_k \leftarrow y_{b,k} - \hat{h}_k$ ;  $Q_k \leftarrow Q_{b,k}$ .
- 13:   **else if** Magnetometer measurement is available **then**
- 14:      $C_{m,k} \leftarrow (29)$ ;  $C_k \leftarrow C_{m,k}$ ;
- 15:      $y_k \leftarrow y_{m,k} - \hat{R}_k \mathbf{m}_{\mathcal{B}_k}$ ;  $Q_k \leftarrow Q_{m,k}$ .
- 16:   **else if** Pitot measurement is available **then**
- 17:      $C_{p,k} \leftarrow (28)$ ;  $C_k \leftarrow C_{p,k}$ ;
- 18:      $y_k \leftarrow y_{p,k} - B^\top \hat{V}_{a,k}$ ;  $Q_k \leftarrow Q_{p,k}$ .
- 19:   **end if**
- 20:   **if**  $y_{p,k}$  or  $y_{b,k}$  or  $y_{m,k}$  or all are available **then**
- 21:      $K_k = P_{k+1|k} C_k^\top (C_k P_{k+1|k} C_k^\top + Q_k)^{-1}$ ;
- 22:      $P_{k+1|k+1} = (I_7 - K_k C_k) P_{k+1|k}$ ;
- 23:      $u_k \leftarrow -K_k y_k$ ;  $\delta_{R,k} \leftarrow u_k(1:3)$ ;  $\delta_{v,k} \leftarrow u_k(4:6)$ ;  
 $\delta_{h,k} \leftarrow u_k(7)$ .
- 24:   **else**
- 25:      $u_k \leftarrow 0$ ;  $P_{k+1|k+1} \leftarrow P_{k+1|k}$ ;  $\delta_{R,k}, \delta_{v,k}, \delta_{h,k} \leftarrow 0$ .
- 26:   **end if**
- 27:      $P_{k+1|k+1} \leftarrow \frac{1}{2}(P_{k+1|k+1} + P_{k+1|k}^\top)$
- 28:      $\hat{R}_{k+1} \leftarrow \hat{R}_k \exp((\boldsymbol{\omega}_k - \hat{R}_k^\top \delta_{R,k})^\times T)$ ;
- 29:      $\zeta_{1,k} \leftarrow -\boldsymbol{\omega}_k^\times \hat{V}_{a,k} + g \hat{R}_k^\top \mathbf{e}_3 + \mathbf{a}_k$
- 30:      $\zeta_{2,k} \leftarrow -\hat{R}_k^\top \delta_{v,k} + \hat{R}_k^\top \delta_{R,k}^\times \hat{R}_k \hat{V}_{a,k}$
- 31:      $\hat{V}_{a,k+1} \leftarrow \hat{V}_{a,k} + T(\zeta_{1,k} + \zeta_{2,k})$ ;
- 32:      $\hat{h}_{k+1} \leftarrow \hat{h}_k + T(\mathbf{e}_3^\top \hat{R}_k \hat{V}_{a,k} - \delta_{h,k})$
- 33: **end for**

---

exponential-Euler and Euler integrations on  $\text{SO}(3) \times \mathbb{R}^3 \times \mathbb{R}$  (Mahony et al., 2008) (see lines 28–32 of Algorithm 1).

## 7. SIMULATION RESULTS

To evaluate the performance of the proposed observer, we conduct a simulation of a vehicle illustrated in fig. 1 equipped with one calibrated Pitot probe and the barometer-IMU system moving in a 3D space. The ground truth inertial velocity and altitude are respectively given by  $v(t) = [-1.5 \sin(1.5t), 3 \cos(3t), -15\sqrt{3} \cos(3t)/4]^\top$  and  $h(t) = -5\sqrt{3} \sin(3t)/4$ . We excite only the yaw component. Hence, the angular velocity is given by  $\boldsymbol{\omega}(t) = [0, 0, 0.7 \sin(1.6t)]^\top$  and the body-frame linear acceleration is given by

$$\mathbf{a}(t) = R^\top \begin{bmatrix} -2.25 \cos(1.5t) \\ -9 \sin(3t) \\ 11.25\sqrt{3} \sin(3t) - g \end{bmatrix}.$$

The pitot geometry is such that  $B = b_1 = \mathbf{e}_1$ . We assume the absence of wind  $v_w \approx 0$  in that 3D space. This implies that the ground truth inertial air-velocity is given by  $v_a \approx v$ . Hence, the ground truth body-frame air-velocity is generated by  $V_a = R^\top v$ . The constant vector  $m_{\mathcal{I}}$  is set to  $m_{\mathcal{I}} = [1/\sqrt{2} \ 0 \ 1/\sqrt{2}]^\top$ .

A Monte Carlo simulation with 20 runs is performed, where the initial estimates are randomly sampled from Gaussian distributions. The initial body-frame air-velocity and the altitude estimates are distributed around  $\hat{V}_a(0) = [10, -2, 8]^\top$  (m/s) per axis and  $\hat{h}(0) = 10$  (m) with a standard deviation of 2 (m/s) and 1 (m), respectively. The initial orientation estimates are normally distributed around  $\hat{R}(0)$  which corresponds to the initial angles with a pitch of  $-\pi/20$  (rad), a roll of  $\pi/20$  (rad), and a yaw of  $\pi/6$  (rad); with a standard deviation of  $\pi/12$  per axis. The parameters are set as follows:  $Q = 100 * \text{blkdiag}(\sigma_{p,1}^2, (\sigma_m^\top)^2, \sigma_b^2)$ ,  $S = \text{blkdiag}(0.01I_3, 0.1I_3, 0.01)$ ,  $P(0) = \text{blkdiag}(0.1I_3, 0.25I_3, 1)$ . The accelerometer and gyroscope measurements  $\mathbf{a}(t)$  and  $\boldsymbol{\omega}(t)$  sampled at 200 (Hz), are corrupted with zero-mean Gaussian noise with standard deviation of 0.05 each. The magnetometer and Pitot measurements in body frame, sampled at 50 (Hz) are corrupted with zero-mean Gaussian noise with standard deviations  $\sigma_m = 0.01 * [1, 1, 1]^\top$ , and  $\sigma_{p,1} = 0.5$ , respectively. The barometer sampled at 5 (Hz), is corrupted with zero-mean Gaussian noise with standard deviation  $\sigma_b = 0.05$ . Figures 3 and 4 illustrate the air-velocity components and full air-velocity estimation error ( $\|V_a - \hat{V}_a\|$ ), and the Euler angles and full attitude estimation error ( $\text{trace}(I_3 - R\hat{R}^\top)$ ). The simulation results demonstrate that the estimation errors decrease and converge to zero under Yaw rate-only motion and forward Pitot measurement. In particular, the full air-velocity and the Euler angles estimates remain bounded with fast convergence for all initial conditions. These results confirm the expected local convergence and robustness properties of the proposed observer.

## 8. CONCLUSION

In this work, we proposed a nonlinear observer on  $\text{SO}(3) \times \mathbb{R}^3 \times \mathbb{R}$  for full air-velocity and attitude estimation, where the innovation terms are systematically derived from a CRE associated with the linearized error dynamics. The theoretical analysis (Lemma 1 and Theorem 2) established a uniform observability of the augmented system and local convergence of the estimation error dynamics under persistently exciting motion. A Monte Carlo simulation with perturbed initial conditions corroborated the analysis, showing consistent convergence of the proposed observer across all runs. Future work will extend the approach to explicitly estimate IMU-biases and wind-dynamic effects.

## Appendix A. PROOF OF LEMMA 1

First, the corresponding observability Gramian is evaluated in a convenient block form. In particular, we block-partition the system matrix  $A^*(t)$  as

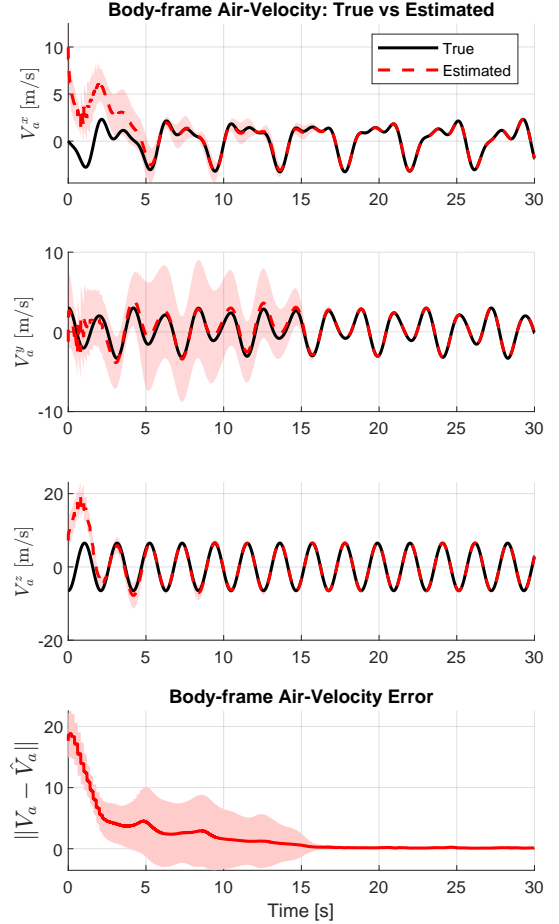


Fig. 3. Estimated and True body-frame air-velocity components, and observer estimation error  $\|V_a - \hat{V}_a\|$ .

$$A^*(t) = \begin{bmatrix} A_{11}^*(t) & \mathbf{0}_{6 \times 1} \\ A_{21} & 0 \end{bmatrix}, \quad (\text{A.1})$$

with

$$A_{11}^*(t) = \begin{bmatrix} \mathbf{0}_{3 \times 3} & \mathbf{0}_{3 \times 3} \\ -(R\mathbf{a})^\times & \mathbf{0}_{3 \times 3} \end{bmatrix}, \quad A_{21} = [\mathbf{0}_{1 \times 3} \ \mathbf{e}_3^\top].$$

Similarly, we block-partition the output matrix  $C^*(t)$  as

$$C^*(t) = \begin{bmatrix} C_{11}^*(t) & \mathbf{0}_{(m+3) \times 1} \\ \mathbf{0}_{1 \times 6} & 1 \end{bmatrix}, \quad (\text{A.2})$$

with

$$C_{11}^*(t) = \begin{bmatrix} B^\top R^\top (RV_a)^\times & B^\top R^\top \\ -(m_{\mathcal{I}})^\times & \mathbf{0}_{3 \times 3} \end{bmatrix}.$$

Due to the structure of  $A^*$  in (A.1), the associated state transition matrix has the block form

$$\Phi^*(t, \tau) = \begin{bmatrix} \Phi_{11}^*(t, \tau) & \mathbf{0}_{6 \times 1} \\ \Phi_{21}^*(t, \tau) & 1 \end{bmatrix}, \quad (\text{A.3})$$

with  $\Phi_{11}^* \in \mathbb{R}^{6 \times 6}$  and  $\Phi_{21}^* \in \mathbb{R}^{1 \times 6}$ . From (22) and (A.3), the derivative of the transition matrix is given by

$$\frac{d}{dt} \Phi^*(t, \tau) = \begin{bmatrix} A_{11}^* \Phi_{11}^* & \mathbf{0}_{6 \times 1} \\ A_{21} \Phi_{11}^* & 0 \end{bmatrix}, \quad \Phi^*(\tau, \tau) = I_7. \quad (\text{A.4})$$

with  $\Phi_{11}^*(\tau, \tau) = I_6$  and  $\Phi_{21}^*(\tau, \tau) = \mathbf{0}_{1 \times 6}$ . From (A.4), we have

$$\dot{\Phi}_{11}^* = A_{11}^* \Phi_{11}^*, \quad (\text{A.5a})$$

$$\dot{\Phi}_{21}^* = A_{21} \Phi_{11}^*. \quad (\text{A.5b})$$

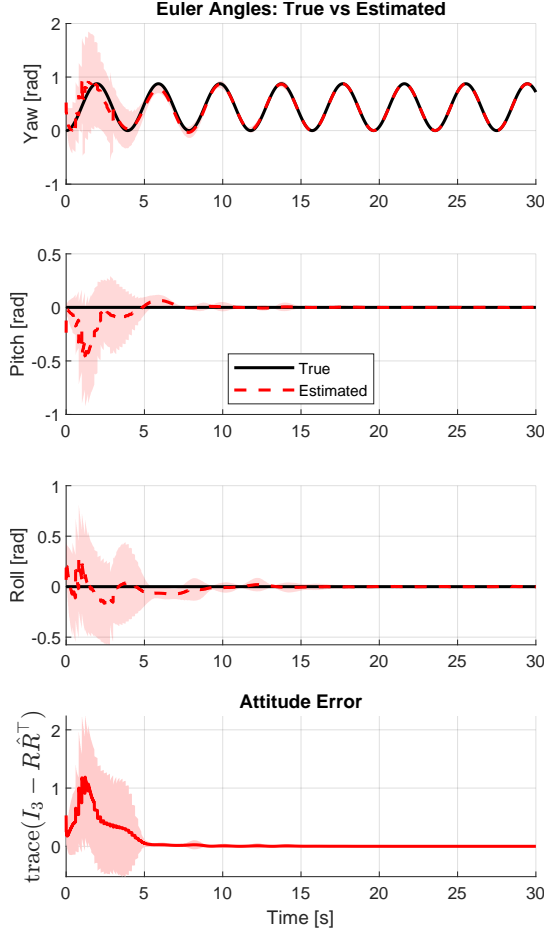


Fig. 4. Estimated and True Euler angles and attitude estimation error  $\text{trace}(I_3 - R\hat{R}^\top)$ .

Due to the structure of  $A_{11}^*$ ,  $\Phi_{11}^*$  is obtained from (A.5a) as follows

$$\Phi_{11}^*(t, \tau) = \begin{bmatrix} I_3 & \mathbf{0}_{3 \times 3} \\ -\int_\tau^t (\mathbf{Ra})^\times(s) ds & I_3 \end{bmatrix}. \quad (\text{A.6})$$

Substituting  $A_{21}$  and (A.6) in (A.5b) yields:

$$\Phi_{21}^*(t, \tau) = \mathbf{e}_3^\top \left[ -\int_\tau^t \left( \int_\tau^s (\mathbf{Ra})^\times d\sigma \right) ds \ I_3(t - \tau) \right]. \quad (\text{A.7})$$

From (A.2) and (A.3), we compute  $C^* \Phi^*$  as follows

$$C^*(s) \Phi^*(s, t) = \begin{bmatrix} C_{11}^*(s) \Phi_{11}^*(s, t) & \mathbf{0}_{(m+3) \times 1} \\ \Phi_{21}^*(s, t) & 1 \end{bmatrix} \quad (\text{A.8})$$

Now, in view of (A.8) and (21), the Gramian is given by

$$W^*(t, t + \bar{\delta}) = \begin{bmatrix} W_{11}^*(t, t + \bar{\delta}) & W_{21}^{*\top}(t, t + \bar{\delta}) \\ W_{21}^*(t, t + \bar{\delta}) & 1 \end{bmatrix} \quad (\text{A.9})$$

where

$$\begin{aligned} W_{11}^*(t, t + \bar{\delta}) &= \frac{1}{\bar{\delta}} \int_t^{t+\bar{\delta}} \Phi_{11}^{*\top} C_{11}^{*\top} C_{11}^* \Phi_{11}^* ds \\ &\quad + \frac{1}{\bar{\delta}} \int_t^{t+\bar{\delta}} \Phi_{21}^{*\top}(s, t) \Phi_{21}^*(s, t) ds, \end{aligned}$$

$$W_{21}^*(t, t + \bar{\delta}) = \frac{1}{\bar{\delta}} \int_t^{t+\bar{\delta}} \Phi_{21}^*(s, t) ds.$$

To show that the system (15) is uniformly observable, it suffices to show that there exist  $\bar{\delta}, \bar{\mu} > 0$  such that (21) holds, i.e.  $W^*(t, t + \bar{\delta}) \geq \bar{\mu} I_7$ ,  $\forall t \geq 0$ , with  $W^*(t, t + \bar{\delta})$  given by (A.9). Assume, for contradiction, that the proposed system is *not* uniformly observable. Then, for every  $\bar{\mu} > 0$  and  $\delta > 0$ , there exists  $t \geq 0$  such that  $W^*(t, t + \delta) < \bar{\mu} I_7$ . Let  $\{\mu_p\}_{p \in \mathbb{N}}$  be a sequence decreasing to zero with  $\mu_p > 0$ , and let  $\bar{\delta} > 0$  satisfy the PE conditions (23) and (24). Then, there exist sequences  $\{t_p\}$  and  $\{\hat{d}_p\}$  such that:  $\hat{d}_p \in \mathcal{D} := \{d \in \mathbb{R}^7 : \|d\| = 1\}$ , the unit sphere in  $\mathbb{R}^7$ , and  $\hat{d}_p^\top W^*(t_p, t_p + \bar{\delta}) \hat{d}_p < \mu_p$ ,  $\forall p \in \mathbb{N}$ . Since  $\mathcal{D}$  is compact, there exists a subsequence of  $\{\hat{d}_p\}$  that converges to some  $d \in \mathcal{D}$ ,  $\|d\| = 1$ . Letting  $p \rightarrow \infty$  and using  $\mu_p \rightarrow 0$  yields the convergence relation from (A.9)

$$\lim_{p \rightarrow \infty} \int_0^{\bar{\delta}} \|C^* \Phi^*(s, t_p) \hat{d}_p\|^2 ds = 0 \quad (\text{A.10})$$

or, by a change of variables with an output function,

$$\lim_{p \rightarrow \infty} \int_0^{\bar{\delta}} \|f_p(s)\|^2 ds = 0, \quad (\text{A.11})$$

where we define

$$\begin{aligned} f_p(t) &:= C^* \Phi^*(t + t_p, t_p) \hat{d}_p \\ &= \begin{bmatrix} C_{11}^* \Phi_{11}^*(t + t_p, t_p) d_1 \\ \Phi_{21}^*(t + t_p, t_p) d_1 + d_2 \end{bmatrix} = \begin{bmatrix} f_{1p}(t) \\ f_{2p}(t) \end{bmatrix}, \end{aligned}$$

where  $d = [d_1^\top, d_2^\top]^\top$  with  $d_1 \in \mathbb{R}^6$ ,  $d_2 \in \mathbb{R}$ . This implies

$$\begin{aligned} \|f_p(t)\|^2 &= \|C_{11}^* \Phi_{11}^* d_1\|^2 + \|\Phi_{21}^* d_1 + d_2\|^2 \\ &= \|f_{1p}(t)\|^2 + \|f_{2p}(t)\|^2. \end{aligned}$$

Hence the convergence relation in (A.11) becomes

$$\lim_{p \rightarrow \infty} \int_0^{\bar{\delta}} \|f_{1p}(s)\|^2 ds = 0, \text{ and} \quad (\text{A.12a})$$

$$\lim_{p \rightarrow \infty} \int_0^{\bar{\delta}} \|f_{2p}(s)\|^2 ds = 0. \quad (\text{A.12b})$$

From (A.5b)-(A.7), we obtain the successive time derivatives of  $f_{2p}(t)$ , as follow :

$$f_{2p}^{(1)}(t) = \mathbf{e}_3^\top \left[ - \int_\tau^t (\mathbf{Ra})^\times ds \ I_3 \right] d_1, \quad f_{2p}^{(2)}(t) = -\mathbf{e}_3^\top (\mathbf{Ra})^\times d_1$$

Using the results of Lemma A.1 of Morin et al. (2017), we deduce:

$$\lim_{p \rightarrow \infty} \int_0^{\bar{\delta}} |f_{2p}^{(k)}(s)|^2 ds = 0, \quad k = 0, 1, 2..$$

Letting  $d_1 = [d_{1,1}^\top, d_{1,2}^\top]^\top$ , with  $d_{1,1} \in \mathbb{R}^3$  and  $d_{1,2} \in \mathbb{R}^3$ , the highest derivative yields

$$f_{2p}^{(2)}(t_p) \rightarrow -\mathbf{e}_3^\top (R(t_p) \mathbf{a}(t_p))^\times d_{1,1} \rightarrow 0 \text{ as } p \rightarrow \infty.$$

This implies in the tangent-space

$$-\mathbf{e}_3^\top (R(t_p) \mathbf{a}(t_p))^\times J \bar{d}_{1,1} \rightarrow 0 \text{ as } p \rightarrow \infty,$$

with  $d_{1,1} = [\bar{d}_{1,1}^\top, \alpha]^\top$ , where  $\bar{d}_{1,1} \in \mathbb{R}^2$  and  $\alpha \in \mathbb{R}$ .

By the PE assumption in (24), this leads to  $\bar{d}_{1,1} = 0$ .

Substituting  $\bar{d}_{1,1} = 0$  into  $f_{2p}^{(1)}(t_p)$ , we get  $\mathbf{e}_3^\top d_{1,2} = 0$ , which implies  $d_{1,2} \in \text{span}\{\mathbf{e}_1, \mathbf{e}_2\}$ , i.e.,  $d_{1,2} = [\bar{d}_{1,2}^\top, 0]^\top$ , where  $\bar{d}_{1,2} \in \mathbb{R}^2$ . Now, substituting  $d_1 = [\alpha \mathbf{e}_3^\top, \bar{d}_{1,2}^\top]^\top$ ,  $C_{11}^*$ , and  $\Phi_{11}^*$  into  $f_{1p}(t)$ , we get  $f_{1p}(t) = \begin{bmatrix} \nu(t) \\ -\alpha (m_I \times \mathbf{e}_3) \end{bmatrix}$ , where

$$\begin{aligned}\nu(t) &= B^\top R^\top (RV_a)^\times \alpha \mathbf{e}_3 \\ &+ B^\top R^\top (-\alpha \int_\tau^t (R\mathbf{a})^\times(s) ds \mathbf{e}_3 + d_{1,2}).\end{aligned}$$

Hence  $f_{1p}(t_p) \rightarrow 0$  as  $p \rightarrow \infty$ , implies  $\alpha(m_{\mathcal{I}} \times \mathbf{e}_3) \rightarrow 0$  and  $\nu(t_p) \rightarrow 0$  as  $p \rightarrow \infty$ . By assumption, vectors  $m_{\mathcal{I}}$  and  $\mathbf{e}_3$  are non-collinear, then  $\alpha \rightarrow 0$  as  $p \rightarrow \infty$ . Thus,  $\nu(t_p) \rightarrow BR^\top d_{1,2} \rightarrow 0$  as  $p \rightarrow \infty$ . Since  $d_{1,2} \in \text{span}\{\mathbf{e}_1, \mathbf{e}_2\}$  and by the PE assumption in (23), this implies  $d_{1,2} = 0$ . Substituting  $d_1 = 0$  into  $f_{2p}(t_p)$ , we get  $d_2 \rightarrow 0$  as  $p \rightarrow \infty$ . Hence  $d = 0$ , contradicting  $\|d\| = 1$ . Therefore, the pair  $(A^*(t), C^*(t))$  is uniformly observable.

## REFERENCES

Barczyk, M. and Lynch, A.F. (2012). Invariant observer design for a helicopter uav aided inertial navigation system. *IEEE Transactions on Control Systems Technology*, 21(3), 791–806.

Barrau, A. and Bonnabel, S. (2019). Linear observed systems on groups. *Systems & Control Letters*, 129, 36–42.

Benallegue, M., Benallegue, A., Cisneros, R., and Chitour, Y. (2023). Velocity-aided imu-based tilt and attitude estimation. *IEEE Transactions on Automatic Control*, 68(10), 5823–5836. doi:10.1109/TAC.2022.3225758.

Berkane, S. and Tayebi, A. (2017). Attitude and gyro bias estimation using gps and imu measurements. In *56th Annual Conference on Decision and Control (CDC)*, 2402–2407. IEEE.

Besançon, G. (2007). *An Overview on Observer Tools for Nonlinear Systems*, 1–33. Springer Berlin Heidelberg, Berlin, Heidelberg.

Bonnabel, S., Martin, P., and Rouchon, P. (2008). Symmetry-Preserving Observers. *IEEE Transactions on Automatic Control*, 53(11), 2514–2526. doi:10.1109/TAC.2008.2006929.

Borup, K.T., Fossen, T.I., and Johansen, T.A. (2016). A nonlinear model-based wind velocity observer for unmanned aerial vehicles. *IFAC-PapersOnLine*, 49(18), 276–283.

Bryne, T.H., Hansen, J.M., Rogne, R.H., Sokolova, N., Fossen, T.I., and Johansen, T.A. (2017). Nonlinear observers for integrated insgnss navigation: Implementation aspects. *IEEE Control Systems Magazine*, 37(3), 59–86. doi:10.1109/MCS.2017.2674458.

de Oliveira, T.L., van Goor, P., Hamel, T., Mahony, R., and Samson, C. (2024). Pitot tube measure-aided air velocity and attitude estimation in gnss denied environment. *European Journal of Control*, 80, 101070. 2024 European Control Conference Special Issue.

Grip, H.F., Fossen, T.I., and Johansen, T.A. (2013). Nonlinear observer for gnss-aided inertial navigation. *Automatica*, 49(1), 108–116.

Hamel, T. and Samson, C. (2017). Riccati observers for the nonstationary pnp problem. *IEEE Transactions on Automatic Control*, 63(3), 726–741.

Hansen, J., Fossen, T.I., and Johansen, T.A. (2017). Nonlinear observer design for gnss-aided inertial navigation systems with time-delayed gnss measurements. *Control Engineering Practice*, 61, 188–197.

Hua, M.D., Hamel, T., and Samson, C. (2017). Riccati nonlinear observer for velocity-aided attitude estimation of accelerated vehicles using coupled velocity measure-ments. In *2017 IEEE 56th Annual Conference on Decision and Control (CDC)*, 2428–2433. IEEE.

Hua, M.D., Martin, P., and Hamel, T. (2016). Stability analysis of velocity-aided attitude observers for accelerated vehicles. *Automatica*, 63, 11–15. doi:10.1016/j.automatica.2015.10.014.

Johansen, T.A., Cristofaro, A., Sørensen, K., Hansen, J.M., and Fossen, T.I. (2015). On estimation of wind velocity, angle-of-attack and sideslip angle of small uavs using standard sensors. In *2015 International Conference on Unmanned Aircraft Systems (ICUAS)*, 510–519. IEEE.

Lageman, C., Trumpf, J., and Mahony, R. (2008). Observer design for invariant systems with homogeneous observations. *arXiv preprint arXiv:0810.0748*.

Lie, F.A.P. (2014). *Synthetic air data estimation*. Ph.D. thesis, university of minnesota.

Ma, Y., Soatto, S., Košecká, J., and Sastry, S.S. (2004). *An Invitation to 3-D Vision: From Images to Geometric Models*, volume 26 of *Interdisciplinary Applied Mathematics*. Springer, New York. doi:10.1007/b97515. Rodrigues' formula derivation in Chapter 2.

Mahony, R., Euston, M., Kim, J., Coote, P., and Hamel, T. (2011). A non-linear observer for attitude estimation of a fixed-wing unmanned aerial vehicle without gps measurements. *Transactions of the Institute of Measurement and Control*, 33(6), 699–717.

Mahony, R., Hamel, T., and Pfleimlin, J.M. (2008). Non-linear complementary filters on the special orthogonal group. *IEEE Transactions on Automatic Control*, 53(5), 1203–1218. doi:10.1109/TAC.2008.923738.

Morin, P., Eudes, A., and Scandaroli, G. (2017). Uniform observability of linear time-varying systems and application to robotics problems. In F. Nielsen and F. Barbaresco (eds.), *Geometric Science of Information*, 336–344. Springer International Publishing, Cham.

Sastry, S. (1999). Lyapunov stability theory. In *Nonlinear systems: analysis, stability, and control*, 182–234. Springer.

Sun, K., Regan, C.D., and Gebre-Egziabher, D. (2019). Observability and performance analysis of a model-free synthetic air data estimator. *Journal of Aircraft*, 56(4), 1471–1486.

Tchonkeu, M.N., Berkane, S., and Hamel, T. (2025). Barometer-aided attitude estimation. URL <https://arxiv.org/abs/2509.13649>. Submitted to ACC 2026.

Troni, G. and Whitcomb, L.L. (2013). Preliminary experimental evaluation of a Doppler-aided attitude estimator for improved Doppler navigation of underwater vehicles. In *IEEE International Conference on Robotics and Automation*, 4134–4140. doi:10.1109/ICRA.2013.6631160.